Illuminating the Complex Role of the Added Mass during Vortex Induced Vibration

Zhicheng Wang (王志成),[1] Dixia Fan (范迪夏)*,[2] and Michael S. Triantafyllou[3]
[1)] *Laboratory of Ocean Energy Utilization of Ministry of Education, Dalian University of Technology, Dalian, 116024, China*
[2)] *Department of Mechanical and Materials Engineering, Queen's University, Kingston, Ontario K7M 3N9, Canada*
[3)] *Massachusetts Institute of Technology, Cambridge, Massachusetts 02139, USA*

(*Electronic mail: dixia.fan@queensu.ca)

(Dated: 25 March 2022)

The role of the added mass coefficient in vortex induced vibration (VIV) of the bluff body is complex and elusive. It is certainly that decoding the relationship between the added mass and vibration pattern will benefit the prediction and prevention of VIV. We present a study on VIV of a long flexible cylinder and forced vibration of a rigid cylinder, in a combination of experimental optical measurements and high-fidelity numerical simulation. We focus on uniform flow over uniform cylinder at a fixed Reynolds number, $Re_d = 900$, but systematically varied the motion amplitude in in-line ($\frac{A_x}{d}$) and cross-flow direction ($\frac{A_y}{d}$), as well as the phase angle (θ) between the motions. We show that $\theta \in [\frac{\pi}{2}, \frac{3\pi}{2}]$ is associated with negative added mass coefficients in cross-flow direction ($C_{my} < 0$) and there is a strong correlation between the vortex shedding mode of "2P" or "P+S" and $C_{my} < 0$.

I. INTRODUCTION

It is well known that the vortices shedding from bluff bodies generate oscillatory forces, which may induce the vibration of the bluff body, if it is flexibly mounted or deformable as a string[1]. This particular fluid structure interaction (FSI) problem is better known as vortex induced vibration (VIV). VIV has significant importance in everyday life and physical applications in the real world, such as cable in the blowing wind or riser in the ocean current. When VIV happens, due to the interaction of the vortex and body (the relative motion varies between the vortex and the body), the effective added mass C_m can vary significantly from a negative value to a large positive value[2–5] and C_m plays complex role in determining the system natural and vibration frequencies[6].

A rigid circular cylinder oscillating only in the cross-flow (CF) direction is one of the simplest model of VIV. It has been established that over a broad range of incoming velocities, different regimes of response can be classified as initial, upper and lower branches for the rigid cylinder CF-only free vibration and distinct vortex shedding modes are identified[7]. Furthermore, by imposing prescribed forced motion and measuring the corresponding fluid forces, the lift coefficients in phase with velocity and added mass coefficients are both strongly correlated to the true reduced velocity $V_r = \frac{U}{fd}$ and non-dimensional CF amplitude $\frac{A_y}{d}$, where U is the incoming velocity, f is the vibration frequency, d is the cylinder diameter and A_y is the prescribed CF vibration amplitude[8]. Detailed flow visualization study[9] established a correlation between the wake pattern and hydrodynamic force, where a slight change of the vibration frequency may result in a sharp change of the magnitude of the oscillatory lift force and the phase between the fluid force and cylinder motion (namely the sign of C_{my}), accompanied with a vortical wake mode switch.

If the cylinder is allowed to move in combined in-line (IL) and CF response[10], considerable differences will be observed in fluid forces, structural responses and wake patterns. In particular, from both rigid cylinder free and forced vibration experiments, the phase θ between the IL and the CF motions is found to have a strong influence on the fluid forces on the oscillating cylinder, Dahl et al.[11] found that positive C_{lv} is strongly associated with a phase angle θ corresponding to a counter-clockwise trajectory. Moreover, the occurrence of high harmonics (3^{rd} harmonics) in the CF direction is also found to be associated with specific values of θ[12]. Although previous studies have highlighted the IL motion have significant impact on CF motion and hydrodynamic forces, to the best of the authors' knowledge, no systematic study has been conducted on the correlation (mapping) between the wake pattern and hydrodynamic force, especially C_{my} for the combined-IL-and-CF rigid cylinder vibration yet.

When the cylinder aspect ratio L/d (L is the cylinder length) becomes larger, the rigid cylinder approximation is no longer held and the model becomes flexible. One of the key differences between rigid and flexible cylinder is that the flexible model obtains multiple structural natural frequencies and vibration modes[13]. It was found that the VIV of the flexible cylinder could happen at a large range of incoming flow velocities and oscillate at different modal numbers. In addition, a large variation of the distribution of the added mass[14] and different wake patterns[15] were observed along the span. Some preliminary results have demonstrated the validity of the strip theory that the rigid cylinder can well capture the fluid force distribution along the flexible cylinder[13], but it is still not clear about the relationship between the the wake pattern and hydrodynamic coefficients, especially the added mass, along the flexible cylinder.

In this paper, we will address the question of the relationship between the added mass coefficient C_{my} and vortical wake pattern behind the rigid and flexible cylinder undergoing VIVs, using the high-fidelity numerical simulation and experimental results. We aim to shed some light on the complex role of the added mass coefficient C_{my} in VIV and its correla-

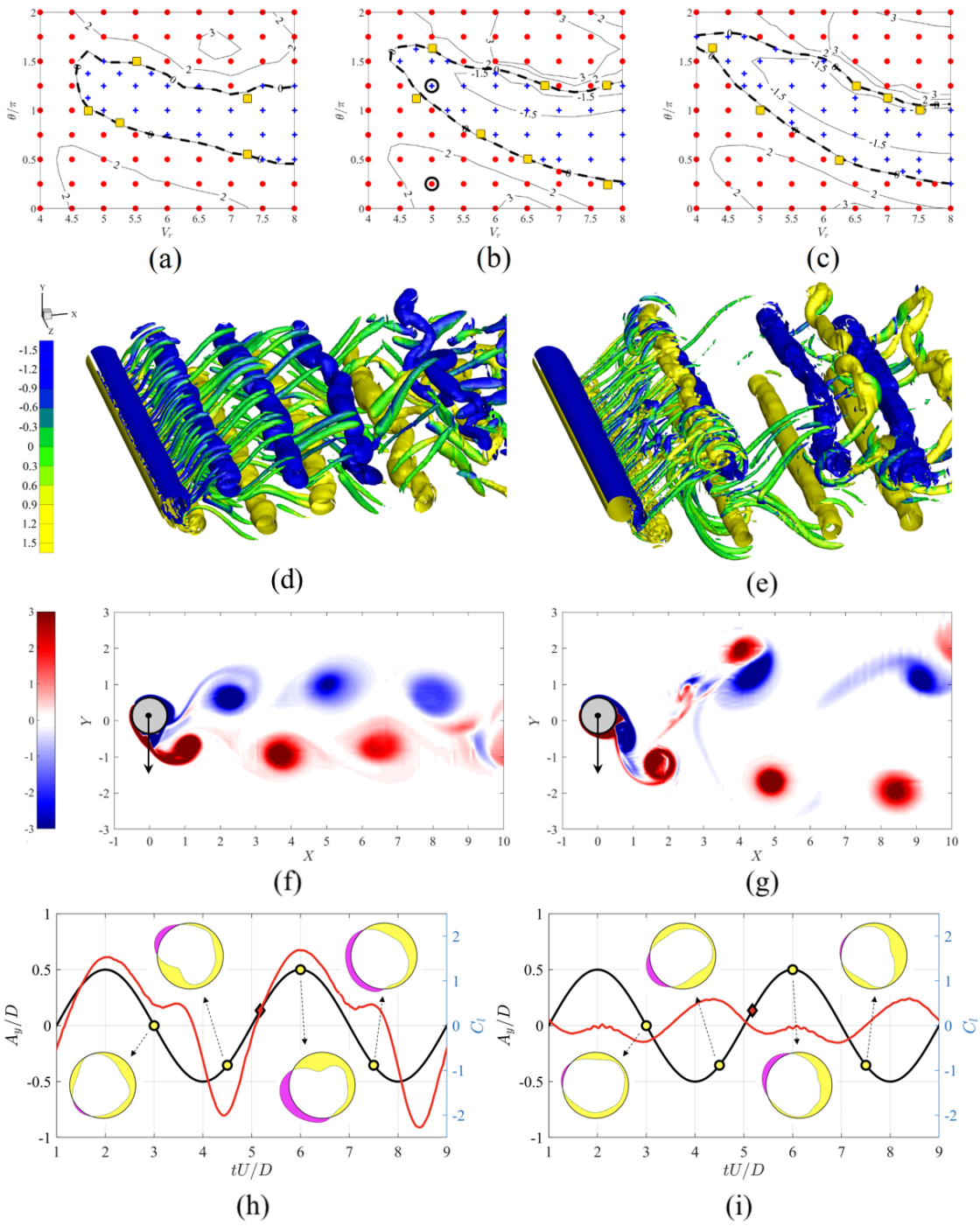

FIG. 1. Simulation results of the forced vibration of a rigid cylinder at $Re = 900$. Figures of the first row, C_{my} map of different amplitude groups: (a) *group 1*: $A_y/d = 0.7$, $A_x/d = 0.1$; (b) *group 2*, $A_y/d = 0.5$, $A_x/d = 0.1$; (c) *group 3*, $A_y/d = 0.5$, $A_x/d = 0.15$. The black bold dashed line highlights $C_{my} = 0$; red dots indicate the stable "2S" vortex mode, the blue crosses represent the stable "P+S" or "2P" vortex mode and the yellow squares denote the unstable vortex mode over 20 cylinder vibration cycles found in the simulation. Figures of the second row, snapshot of the *three dimensional* vortices of *group 2* (corresponding to the red diamonds shown in (h) and (i).): (d) "2S" mode, $V_r = 5$ and $\theta = 0.25\pi$; (f) "P+S" mode, $V_r = 5$ and $\theta = \frac{5\pi}{4}$, corresponding to the two blank circles in Fig. (b). Figures of the third row, snapshot of the *two-dimensional* vorticity field at spanwise location $z/L = 0.5$: (f) "2S" mode, a slice of the vorticity field in Fig.(d); (g) "P+S" mode, a slice of that in Fig.(e). Note that vortices in Fig. (d) and (e) are represented by iso-surfaces of $Q = 0.5$ and colored by ω_z, and the black arrow denotes the acceleration direction of the cylinder. Figures of the fourth row: time history of the CF motion and lift coefficient: (h) case $V_r = 5$ and $\theta = 0.25\pi$; (i) $V_r = 5$ and $\theta = 1.25\pi$. the inset of figures show the instantaneous pressure coefficient $C_p = \frac{p-p_0}{0.5\rho U^2}$ distribution along the cylinder, of which the pink color denotes the positive pressure region and the yellow color denotes the negative pressure region, and magnitude of the unit C_p corresponds to length of $d/8$.

tion with the unique vortical wake patterns.

II. SIMULATION AND EXPERIMENT METHODS

We start with the simulation of the forced vibration of a rigid cylinder of aspect ratio (L/d) 4π and in a uniform oncoming flow, at Reynolds number[16] (Re_d) 900. The motion of the rigid cylinder is prescribed as follows,

$$\begin{cases} y(t) = \frac{A_y}{d} cos(\omega t) \\ x(t) = \frac{A_x}{d} cos(2\omega t + \theta) \end{cases}, \tag{1}$$

where A_x and A_y are the cylinder IL and CF amplitudes, respectively. $\omega = 2\pi f$ is the cylinder vibration frequency and θ is the phase between the IL and CF trajectories. In total 273 simulations have been carried out, which can be divided into three groups, namely *group* 1, $\frac{A_x}{d} = 0.1$ and $\frac{A_y}{d} = 0.7$, *group* 2, $\frac{A_x}{d} = 0.1$ and $\frac{A_y}{d} = 0.5$, *group* 3, $\frac{A_x}{d} = 0.15$ and $\frac{A_y}{d} = 0.5$. Moreover, V_r is in the regime of $[4,8]$ and θ is in the regime of $[0,2\pi]$. Therefore, the added mass coefficient in the CF direction (C_{my}) and the lift coefficient in phase with velocity (C_{lv}) for the rigid cylinder can be calculated as follows,

$$\begin{aligned} C_{my} &= -\frac{2U^2}{\pi d^2} \cdot \frac{\int_{T_s}(C_l(t)\ddot{y}(t))dt}{\int_{T_s}(\ddot{y}^2(t))dt} \\ C_{lv} &= \frac{2}{T_s} \cdot \frac{\int_{T_s}(C_l(t)\dot{y}(t))dt}{\sqrt{\frac{2}{T_s}\int_{T_s}(\dot{y}^2(t))dt}} \end{aligned}, \tag{2}$$

where C_l is the instantaneous lift coefficient, T_s is one vibration cycle. For the flexible cylinder, the distribution of C_{my} along the span hence can be calculated as follows,

$$\begin{aligned} C_{my}(z) &= -\frac{2U^2}{\pi d^2} \cdot \frac{\int_{T_s}(C_l(z,t)\ddot{y}(z,t))dt}{\int_{T_s}(\ddot{y}^2(z,t))dt} \\ C_{lv}(z) &= \frac{2}{T_s} \cdot \frac{\int_{T_s}(C_l(z,t)\dot{y}(z,t))dt}{\sqrt{\frac{2}{T_s}\int_{T_s}(\dot{y}^2(z,t))dt}} \end{aligned}, \tag{3}$$

where z is the location along the flexible model.

In addition, experiments and simulations have been conducted on a tension (varies linearly along the span) dominated flexible beam (string) with a uniform circular cross section, pinned at both ends and free to move in both the IL (x) and CF (y) directions. The flexible cylinder is placed in a uniform oncoming flow with velocity U parallel to the x axis. It is worth noting that the simulations and experiments have exactly same parameters: L/d is 240, structure-to-fluid mass ratio (m^*) is 4.0, damping ratio (ξ) is 0.087, the nominal reduced velocity[17] (U_r) is 17.22 and Re is 900.

Numerically, the complex *three-dimensional* flow past the the vibrating cylinder is obtained by large-eddy simulation (LES), which is based on the entropy viscosity method (EVM)[18] developed and implemented on a spectral *hp* element code[19]. The experiment is conducted at MIT Tow Tank Lab that employs an array of high speed cameras. Note that in the experiments, the time series of the structure displacements are measured at 51 points in both the IL and CF directions along the span and the fluid forces distribution are determined by the inverse force reconstruction method (A complete description of the experimental apparatus and methods is given in[14].). In this paper, the analyzed experimental and numerical results are over 20 stable CF oscillation cycles.

III. RESULTS

Fig. 1 (a) -(c) show the added mass coefficient in the CF direction (C_{my}) as a function of V_r (horizontal axis) and θ (vertical axis) in the three selected *groups* of $\frac{A_x}{d}$ and $\frac{A_y}{d}$. It is found that C_{my} can be both positive and negative in the current V_r - θ range, and the negative C_{my} is consistently found strongly associated with the phase θ, i.e. the cylinder orbits. Specifically, the negative C_{my} favors $\theta \in [\frac{\pi}{2}, \frac{3\pi}{2}]$. However, for the current selected amplitude combinations, the effect of $\frac{A_x}{d}$ and $\frac{A_y}{d}$ on C_{my} is not as prominent as that of V_r and θ.

The value of the added mass coefficient reflects the relative motion between the oscillating cylinder and shedding vortex in the near wake. As shown in the snapshot of the 3D vortical wake in Fig. 1 (d) and (e) and the middle sliced 2D vortical wake in Fig. 1 (f) and (g) for two selected cases (corresponding to the circles in Fig. 1 (b)), different dominant vortex modes, both "P+S" ("2P") and "2S" modes, are observed for different prescribed motions.

For every simulation, we have observed over the wake variation over 20 oscillation cycles, and classify the modes that is highlight them in Fig. 1 (a) - (c). The red circle denotes the stable "2S" vortex mode, shown in Fig. 1 (d) and (f), the blue cross denotes the stable "P+S" or "2P" vortex mode, shown in Fig. 1 (e) and (g), and the yellow square denotes the unstable vortex shedding mode. In current selected IL and CF amplitude combinations, it is clear that there is a strong correlation between the sign of the negative C_{my} and cylinder vortical wake mode: when C_{my} is negative or close to zero, the cylinder wake is dominated by either "P+S" or "2P" vortex mode; when C_{my} is positive, classical "2S" von Kármán appears; close to $C_{my} = 0$, unstable vortex mode (switch between "2S" and "P+S") can be found.

To reveal the detailed flow physics of this phenomenon, from the simulations of *group 2*, we select case of $V_r = 5$ and $\theta = \frac{\pi}{4}$ and plot in Fig. 1 (d) and (f) the snapshots of the "2S" vortex mode. Fig. 1 (e) and (g) exhibit the "P+S" vortex mode corresponding to $V_r = 5$ and $\theta = \frac{5\pi}{4}$. The difference on relative motion between the cylinder and vortex could clearly be observed: in Fig. 1 (f), when the cylinder reaches $y(t_0) = 0.14\frac{A_y}{d}$ from the balance position to the maximum positive position in the CF direction, the vortex (low pressure) appears at the back-side of the cylinder with respect to the cylinder acceleration direction. The time histories of the cylinder motion and lift coefficient are shown in Fig. 1 (h). It is found that the force of a large magnitude is mainly in-phase with the motion, which results in large positive added mass coefficient; on the contrary, as seen from Fig. 1 (h), when "P+S" pattern appears, the small value lift force is out-of-phase with

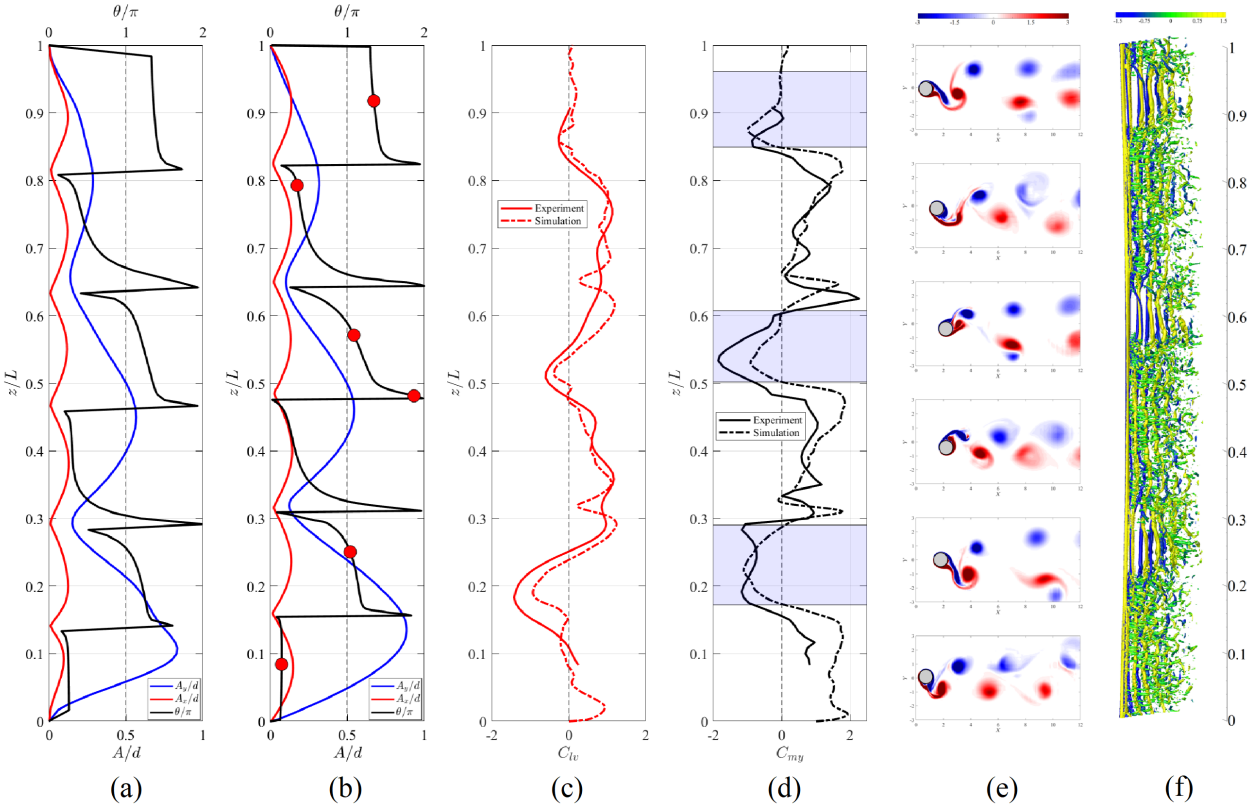

FIG. 2. (color online). Structural response and wake flow of the uniform flexible cylinder ($L/d = 240$) in the uniform current at $Re = 900$. (a) *Experiment result*: blue solid line, CF displacement; red solid line, IL displacement; black solid line, phase angle between IL and CF trajectories (θ); black dashed line, $\theta = \pi$. (b) *Simulation result*: lines are equivalent to (a). (c) Distribution of lift coefficient in phase with velocity (C_{lv}): red solid line, experiment; red dotted line, simulation; black dashed line, $C_{lv} = 0$. (d) Distribution of added mass coefficient in the CF direction (C_{my}): black solid line, experiment; black dotted line, simulation; black dashed line, $C_{my} = 0$; the blue shade highlights the region of "P+S" vortex shedding mode. (e) *Two-dimensional* snapshots of the vorticity field at six spanwise locations highlighted by the red circles in (b): from top to bottom, $z/L = 0.9178$, $z/L = 0.7926$, $z/L = 0.5714$, $z/L = 0.4814$, $z/L = 0.2505$ and $z/L = 0.0842$. (f) A *three-dimensional* snapshot of the vortices. Note that the vortices are represented by iso-surfaces of $Q = 0.1$ and colored by ω_z.

the motion, resulting in a small negative C_{my}. As shown in Fig. 1 (g) for the "P+S" vortex mode, when the cylinder arrives at position $y(t_0) = 0.14\frac{A_y}{d}$ from the balance point to the maximum positive displacement in the CF direction, vortices appear in the front-side of the cylinder relative to the cylinder acceleration direction. In addition, four instantaneous pressure coefficient C_p distributions along the cylinder are plotted for both cases, demonstrating large variation of the pressure around the cylinder when the vortex mode is different.

Unlike the forced vibration of a rigid cylinder, a uniform flexible cylinder in uniform flow may have different vibration patterns, i.e., different $\frac{A_x}{d}$ $\frac{A_y}{d}$ and θ along the span, hence the hydrodynamic coefficients as well as the wake pattern may differ significantly at different locations along the flexible cylinder.

Fig. 2 (a) displays the experiment results of the IL and CF vibration amplitudes as well as θ distribution along the flexible cylinder, and Fig. 2(b) shows the corresponding simulation result. It could be identified that the CF vibration is a mixture of traveling and standing wave, while the IL vibration is dominated by the standing wave. Same as the observation by[20], θ varies continuously in half wavelength of the IL vibration mode and jumps abruptly at the IL nodes . Moreover, positive C_{lv} that implies a net positive energy transfer from the fluid to the structure in the CF direction, is primarily associated with the CCW cylinder orbits, align with the finding in rigid[10] and flexible cylinders[21]. Note that in order to fully validate the simulation result, the comparison of C_{lv} and C_{my} with that of the experiment is shown in Fig. 2 (c) and (d), respectively. Interestingly, similar to the forced vibration of a rigid cylinder, the negative C_{my} distribution of the free vibration of the flexible cylinder is also associated with $\theta \in [\frac{\pi}{2}, \frac{3\pi}{2}]$ region along the span. The local wake pattern behind the cylinder is shown in Fig. 2 (e), which consists of snapshots of the cylinder motion and shedding vortex pattern at six axial positions that are marked out by red dots in Fig. 2 (b). It could be observed that negative C_{my} is strongly correlated to the "P+S" vortex mode (no "2P" mode is found in current flexible cylinder simulation.), while "2S" vortex mode is found where $C_{my} > 0$. Furthermore, as shown in Fig. 2 (f),

accompanying the vortex pattern switching between “2S" and “P+S" along the span, the wake behind the cylinder exhibits two patterns and it can be divided into 6 zones separated by the IL nodes. These two patterns correspond to one region of clear straight vortex tubes and the other one of wavy vortex tubes with strong stream-wise vortices. Note that the “P+S" vortex mode region is highlighted by blue shade in Fig. 2 (d).

IV. DISCUSSION AND CONCLUSION

One of the notable conclusions from previous researches on the vortex induced vibrations of both the flexibly mounted rigid cylinder[11] and flexible cylinder[21] is that the phase difference between the cylinder motion in-line and cross-flow θ alters the strength of the shedding vortices and its timing relative to the cylinder motion. Specifically, the cylinder CCW trajectory ($\theta \in [0, \pi]$) is found to favor positive energy-in from the ambient fluid to the oscillating structure. Our experimental measurements and numerical simulation of the flexible cylinder placed in the uniform inflow further demonstrates that such a phase difference for the cylinder orbit orientation affects the cross-flow added mass (C_{my}) as well. In general, $C_{my} < 0$ is a result of the out-of-phase between the cylinder motion and the vortex force, and is found largely associated with $\theta \in [\frac{\pi}{2}, \frac{3\pi}{2}]$. In addition, strong correlation is observed between the vortex shedding mode of “2P" or “P+S" and $C_{my} < 0$, and therefore, a strong correlation between the cylinder orbit orientation and the wake mode exists as well. Such a relationship is also identified in the simulation of a forced vibrating rigid cylinder with prescribed in-line and cross-flow motions.

In summary, by finding the strong correlation among the sign of the cross-flow added mass, the cylinder orbit orientation and the vortex shedding mode from the rigid and flexible cylinders vibrate in the uniform inflow, our study helps to illuminate the role of the added mass coefficient in bluff body VIVs. Nevertheless, as a fundamental fluid-structure interaction problem, there are many more new phenomena and mechanism that need to be explored and explained. For example, it appears that the IL motion plays an essential role to determine a large variation of hydrodynamic coefficients, even a small IL amplitude may significantly change the instant separation point around the cylinder, and subsequently change the vortex shedding pattern. To this end, more systematic researches are needed in the future to study effect of different motion parameters on the hydrodynamic coefficients and vortical wake patterns of the bluff body undergoing VIVs.

ACKNOWLEDGMENTS

The authors would like to acknowledge the computation resources provided by Compute Canada. In addition, Dixia Fan wish to acknowledge the funding support of the research initiation grant provided by Queen’s University, and Zhicheng Wang wish to acknowledge the support by the Fundamental Research Funds for the Central Universities (DUT21RC(3)063).

DATA AVAILABILITY STATEMENT

The data that supports the findings of this study are available within the article

[1] J. Wang, D. Fan, and K. Lin, “A review on flow-induced vibration of offshore circular cylinders,” Journal of Hydrodynamics **32**, 415–440 (2020).
[2] D. Fan and M. S. Triantafyllou, “Vortex-induced vibration of riser with low span to diameter ratio buoyancy modules,” in *The 27th Inter. Offshore and Polar Eng. Conf* (International Society of Offshore and Polar Engineers, 2017).
[3] D. Fan, G. Jodin, T. Consi, L. Bonfiglio, Y. Ma, L. Keyes, G. E. Karniadakis, and M. S. Triantafyllou, “A robotic intelligent towing tank for learning complex fluid-structure dynamics,” Science Robotics **4** (2019).
[4] K. Lin, D. Fan, and J. Wang, “Dynamic response and hydrodynamic coefficients of a cylinder oscillating in crossflow with an upstream wake interference,” Ocean Engineering **209**, 107520 (2020).
[5] K. Lin, J. Wang, D. Fan, and M. S. Triantafyllou, “Flow-induced cross-flow vibrations of long flexible cylinder with an upstream wake interference,” Physics of Fluids **33**, 065104 (2021).
[6] B. Liu and H. Zhu, “Secondary lock-in of vortex-induced vibration and energy transfer characteristics of a vibrating cylinder subject to cross buoyancy,” Physics of Fluids **33**, 073607 (2021).
[7] C. H. K. Williamson and A. Roshko, “Vortex formation in the wake of an oscillating cylinder,” J. Fluids Struct. **2**, 355–381 (1988).
[8] R. Gopalkrishnan, *Vortex-induced forces on oscillating bluff cylinders*, Ph.D. thesis, Massachusetts Institute of Technology (1993).
[9] J. Carberry, J. Sheridan, and D. Rockwell, “Controlled oscillations of a cylinder: forces and wake modes,” J. Fluid Mech. **538**, 31–69 (2005).
[10] J. M. Dahl, F. S. Hover, M. S. Triantafyllou, and O. H. Oakley, “Dual resonance in vortex-induced vibrations at subcritical and supercritical reynolds numbers,” J. Fluid Mech. **643**, 395–424 (2010).
[11] J. M. Dahl, F. S. Hover, M. S. Triantafyllou, S. Dong, and G. E. Karniadakis, “Resonant vibrations of bluff bodies cause multivortex shedding and high frequency forces,” Phys. Rev. Lett. **99**, 144503 (2007).
[12] J. M. Dahl, F. S. Hover, and M. S. Triantafyllou, “High harmonic forces and predicted vibrations from forced in-line and cross-flow cylinder motions,” in *The 18th Inter. Offshore and Polar Eng. Conf* (International Society of Offshore and Polar Engineers, 2008).
[13] Z. Wang, D. Fan, M. S. Triantafyllou, and G. E. Karniadakis, “A large-eddy simulation study on the similarity between free vibrations of a flexible cylinder and forced vibrations of a rigid cylinder,” Journal of Fluids and Structures **101**, 103223 (2021).
[14] D. Fan, *Mapping the hydrodynamic properties of flexible and rigid bodies undergoing vortex-induced vibrations*, Ph.D. thesis, Massachusetts Institute of Technology (2019).
[15] F. J. Huera-Huarte and P. W. Bearman, “Wake structures and vortex-induced vibrations of a long flexible cylinder—part 1: dynamic response,” J. Fluids Struct. **25**, 969–990 (2009).
[16] The Reynolds number $Re_d = \frac{Ud}{\nu}$ where ν is the fluid kinematic viscosity.
[17] The nominal reduced velocity $U_r = \frac{U}{f_{n1}d}$ where f_{n1} is the natural frequency of the cylinder first vibration mode in the still water, assuming uniform added mass distribution along the span of $C_m = 1.0$.
[18] Z. Wang, M. S. Triantafyllou, Y. Constantinides, and G. M. Karniadakis, “An entropy-viscosity large eddy simulation study of turbulent flow in a flexible pipe,” J. Fluid Mech. **859**, 691–730 (2019).
[19] G. E. Karniadakis and S. Sherwin, *Spectral/hp Element Methods for Computational Fluid Dynamics, 2nd edition* (Oxford University Press, Oxford,UK, 2005).
[20] R. Bourguet, G. E. Karniadakis, and M. S. Triantafyllou, “Phasing mechanisms between the in-line and cross-flow vortex-induced vibrations of a long tensioned beam in shear flow,” Comput. Struct. **122**, 155–163 (2013).
[21] R. Bourguet, Y. Modarres-Sadeghi, G. E. Karniadakis, and M. S. Triantafyllou, “Wake-body resonance of long flexible structures is dominated by counterclockwise orbits,” Phys. Rev. Lett. **107**, 134502 (2011).